

Research Article

Open Access



Improved atom probe specimen preparation by focused ion beam with the aid of multi-dimensional specimen control

Limei Yang¹ , Eason Yi-Sheng Chen^{2,3,8}, Jiangtao Qu², Magnus Garbrecht², Ingrid E. McCarroll⁴, Daniel S. Mosiman⁵, Bivas Saha^{6,7}, Julie M. Cairney^{2,3}

¹School of Civil & Environmental Engineering, University of Technology Sydney, Sydney 2007, Australia.

²Sydney Microscopy and Microanalysis, The University of Sydney, Sydney 2006, Australia.

³School of Aerospace, Mechanical and Mechatronic Engineering, The University of Sydney, Sydney 2007, Australia.

⁴Max-Planck-Institut für Eisenforschung, Düsseldorf 40237, Germany.

⁵Safe Global Water Institute, Department of Civil and Environmental Engineering, University of Illinois at Urbana-Champaign, Urbana, IL 61801, USA.

⁶Chemistry and Physics of Materials Unit and International Centre for Materials Science, Jawaharlal Nehru Centre for Advanced Scientific Research, Bangalore 560064, India.

⁷School of Advanced Materials, Jawaharlal Nehru Centre for Advanced Scientific Research, Bangalore 560064, India.

⁸School of Materials Science and Engineering, Nanyang Technological University, Singapore 639798, Singapore.

Correspondence to: Prof. Julie M. Cairney, School of Aerospace, Mechanical and Mechatronic Engineering, The University of Sydney, 225 Shepherd St, Sydney 2007, Australia. E-mail: julie.cairney@sydney.edu.au; Dr. Limei Yang, School of Civil & Environmental Engineering, University of Technology Sydney, 15 Broadway Street, Sydney 2007 Australia. E-mail: limei.yang@uts.edu.au

How to cite this article: Yang, L.; Chen, E. Y. S.; Qu, J.; Garbrecht, M.; McCarroll, I. E.; Mosiman, D. S.; Saha, B.; Cairney, J. M. Improved atom probe specimen preparation by focused ion beam with the aid of multi-dimensional specimen control. *Microstructures* 2025, 5, 2025007. <https://dx.doi.org/10.20517/microstructures.2024.53>

Received: 27 Jun 2024 **First Decision:** 26 Aug 2024 **Revised:** 4 Oct 2024 **Accepted:** 11 Nov 2024 **Published:** 23 Jan 2025

Academic Editors: Yi Du, Lin Gu **Copy Editor:** Ping Zhang **Production Editor:** Ping Zhang

Abstract

Focused ion beam lift-out has become an essential technique for fabricating small-scale specimens in atom probe tomography (APT). By using a rotatable micromanipulator, we developed methods that can precisely extract the regions of interest for APT samples with challenging-to-prepare geometries. Combining this function with pre-milling and pre-tilt operations, we prepare three typically challenging APT specimens: nanoparticles, nanowires, and thin films. This combination can effectively decrease the sample preparation time and increase the accuracy of focused ion beam lift-out specimen preparation.

Keywords: Focused-ion beam, atom probe tomography, microanalysis, nanomaterials



© The Author(s) 2025. **Open Access** This article is licensed under a Creative Commons Attribution 4.0 International License (<https://creativecommons.org/licenses/by/4.0/>), which permits unrestricted use, sharing, adaptation, distribution and reproduction in any medium or format, for any purpose, even commercially, as long as you give appropriate credit to the original author(s) and the source, provide a link to the Creative Commons license, and indicate if changes were made.



INTRODUCTION

Focused ion beam (FIB) lift-out is commonly used for the fabrication of the tiny samples required for high-resolution materials characterization techniques such as atom probe tomography (APT) or transmission electron microscopy (TEM). FIB lift-out procedures generally start with the use of ion beams to carve out a region of interest (ROI) from a bulk specimen surface in a scanning electron microscope (SEM)^[1-3]. Then, a micromanipulator, which is usually a sharpened tungsten tip, is inserted and attached to the ROI by using conductive deposition, enabled by a localized gas-injection system (GIS) and the secondary electrons generated from the incident electron beam or ion beam. After attachment, the micromanipulator is withdrawn, lifting out an ROI that includes features of interest, such as second phases, interfaces, or grain boundaries. After lift-out, the sample segment is attached to a sample carrier configured specifically for the subsequent microscopy analysis, such as a TEM grid or an APT pre-sharpened post^[1-3]. Finally, the sample segment is ion-milled into the geometry required for analyses by the particular microscopy technique^[4].

APT is a powerful technique that can provide quantitative analysis with both high spatial and chemical resolutions^[4-7]. An APT specimen is required to be an ultra-sharp tip with a diameter of hundreds of nm. The sharp tip enables a strong electric field to be generated at its apex when a high voltage is applied. When the generated field is large enough, field-ionization of the apex atoms ensues. This electric field is applied by time-controlled pulsing, and the ions are detected by a device that is sensitive to both the time and position of incoming ions. The time-of-flight of evaporated ions provides information as to their chemical identities, and the position of the atoms on the detector allows the determination of their spatial origins via a back-projection model^[8,9]. The ions with their chemical identities, (x, y) positions and the order of arrival can then be reconstructed into a three-dimensional (3D) atom map that typically has a volume of up to $100 \times 100 \times 500 \text{ nm}^3$ ^[4]. One approach is to encapsulate the small samples into a suitable bulk support which can then be fabricated into the required APT geometry^[10-18]. However, the throughput of such analysis using conventional FIB lift-out protocols has been low because precisely aligning buried objects within the limited field of view (FOV) of APT is not straightforward^[11]. Also, weak bonding between the nano-objects and encapsulation materials can lead to specimen failure when exposed to the strong electric fields required for field ionization. As such, new protocols are needed to address challenges associated with fabrication of robust nano-objects for APT analysis by FIB lift-out.

While gallium-sourced FIB has been in use for many years, plasma FIB is now widely employed for APT sample preparation with its increasing success rate^[19,20]. In this work, we have used the Thermo Scientific EasyLift nanomanipulator with in-situ rotation control, adding another degree of freedom for sample manipulation on top of the existing 5- and 3-axial movements for the sample stage and manipulator, respectively. Rotating the manipulator allows in-situ adjustments of specimen orientation and ion-mill direction of lift-out bars, and this new function is useful for precisely targeting nano-objects^[17]. In this work, we successfully combine this function together with pre-milling and pre-tilt to prepare three typically challenging APT specimens: nanoparticles, nanowires, and thin films. This combination can effectively decrease the sample preparation time and increase the accuracy of FIB lift-out specimen preparation.

MATERIALS AND METHODS

As illustrated in [Figure 1](#), central to this work is that a rotatable manipulator allows an attached lift-out bar to be rotated in-situ 90 degrees with respect to the original orientation, which is achieved by rotating the manipulator 180 degrees. This maneuver requires a 45-degree pre-angled attachment of the manipulator to the sample surface [[Figure 1A](#)], to enable a perpendicular orientation of the lift-out bar to the original sample surface [[Figure 1B](#)]. Note that the front and back sides of the sample in [Figure 1A](#), noted as 1 and 2,

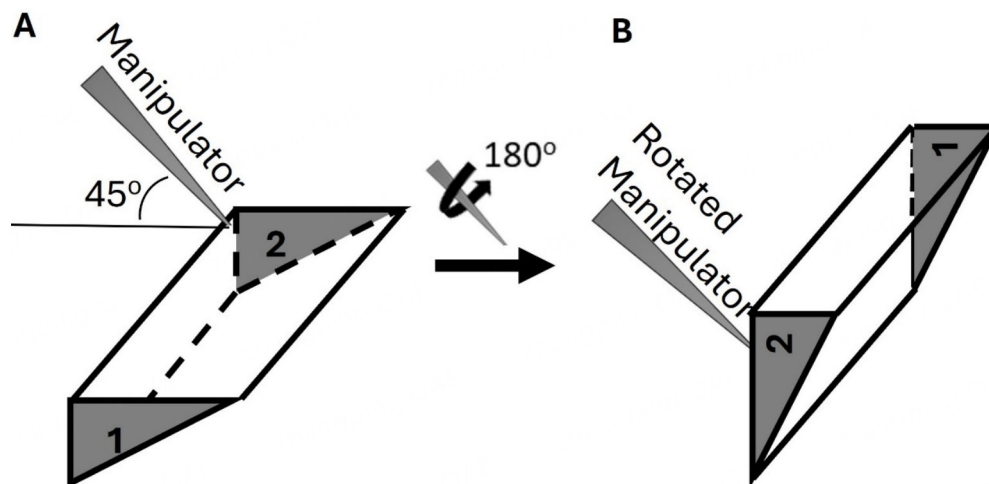


Figure 1. Schematic illustrations of how to change the orientation of lifted-out bar using the rotatable manipulator fitted in PFIB. The relative orientations of manipulator and the lifted-out bar (A) before and (B) after rotation. PFIB: Plasma focused ion beam.

respectively, are reversed in Figure 1B after the rotation. In this work, a Thermo Fisher G4 Helios Hydra plasma FIB (PFIB) was employed for sample manipulations and APT tip fabrications, and a CAMECA LEAP4000 X Si was used for APT experiments. APT data reconstruction and analysis were performed using the commercial software AP Suite 6.1.

This paper focuses on three different types of nanostructured materials, including nanoparticles, nanowires and thin films. Due to the distinct dimensions and orientations of these materials, the procedures of FIB preparations are slightly different. Information and results are therefore discussed separately in the next section.

RESULTS AND DISCUSSION

Encapsulated nanoparticles

Encapsulating nanoparticles into tips is a feasible route for analyzing nanoparticles in APT, allowing atomic-scale observation of the chemical heterogeneity of individual nanoparticles^[21–25]. Preparing an APT tip with encapsulated nanoparticles typically involves: (1) dispersing nanoparticles onto a flat substrate with an adequate number density and minimum agglomeration; (2) deposition of an encapsulation coating, ideally using the same material as the substrate to minimize aberrations in the APT reconstruction due to the intrinsic difference between encapsulation/substrate evaporation fields^[11]; (3) a FIB lift-out and attachment process that allows the substrate/coating interface to be aligned along the APT analysis direction to minimize the electrostatic force applied at the interface, which is susceptible to failure^[22]. In this work, two example encapsulations for calcium hydroxyapatite [$\text{Ca}_5(\text{PO}_4)_3\text{OH}$, HAP] nanoparticle samples were used, one with atomic layer deposition (ALD) of alumina (Al_2O_3) on a substrate of the same material and another with sputter-coated gold (Au) doped with traceable silver (Ag) on a Au substrate. Details of the dispersion and encapsulation methods are provided^[25].

As shown in Figure 2A, after the dispersion and encapsulation of the nanoparticles, a 1- μm platinum (Pt) protective layer was deposited onto the surface before the lift-out bar was attached to the manipulator. Note that the FIB trenching configuration here is different from conventional FIB lift-out wedges to allow for a lift-out bar that can incorporate more encapsulated layers^[2]. Next, as shown in Figure 2B, the bar was lifted away from the bulk sample and a pre-milling process was applied to the thinner side of the bar. After

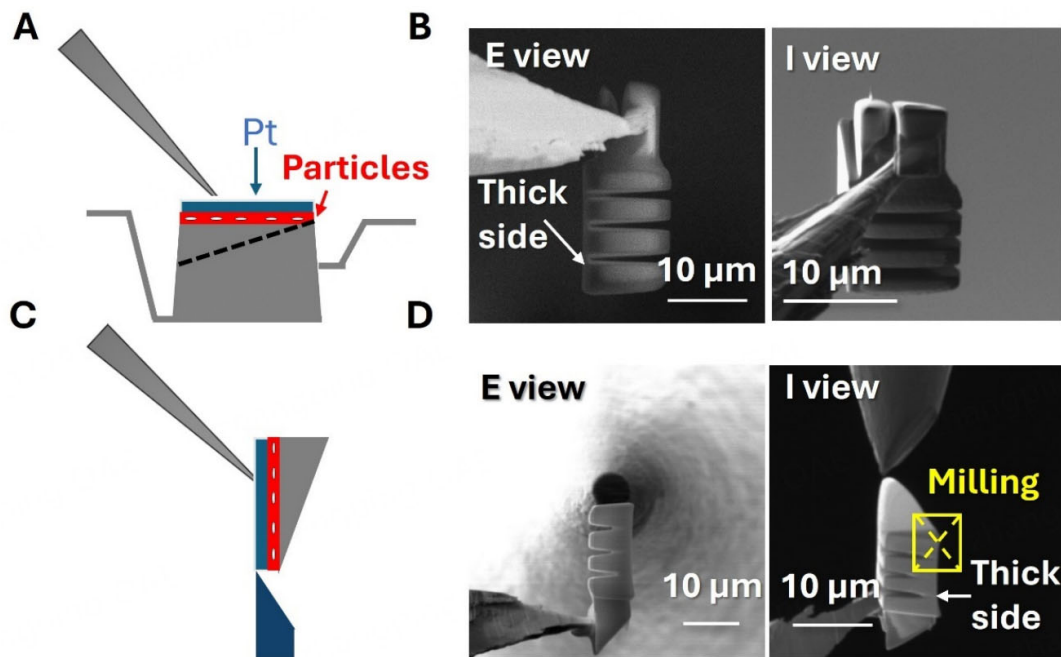


Figure 2. (A) Schematic illustration of lifting out a bar with encapsulated NPs; (B) Electron imaging and Ion imaging of lifted-out bar before rotating the manipulator; (C) schematic illustration showing the lifted-out wedge after 180° rotation of the manipulator; (D) Electron and Ion imaging of the lifted-out bar after rotating the manipulator for 180° and the alignment between the bar and the pre-sharpened tungsten post for attaching. NPs: Nanoparticles.

rotating the manipulator with the lift-out bar by 180°, the encapsulation layer became parallel to the pre-sharpened post [Figure 2C]. As shown in Figure 2D, the pre-milling facilitates the detachment of the sample wedges, which have the milling pattern on the thick side connecting the wedge and the bar. The combination of pre-milling and manipulator rotation effectively decreases preparation time and simplifies the procedure.

The ALD Al_2O_3 encapsulation tip was tested in laser-pulsing mode at 50 K and 100 kHz pulse frequency with 60 pJ laser energy, the results of which are shown in Figure 3A, which shows a 3D reconstruction of the APT data with Al ions and 3.4 at.% isoconcentration surfaces (isosurfaces), representing the locations of the encapsulated HAP nanoparticles. The result shows that the nanoparticle sample fabrication method has successfully yielded multiple nanoparticles in a single APT dataset. In order to confirm that the nanoparticle is captured at the interface, another experiment using a Au substrate and a Ag-doped Au sputter coating was conducted in voltage-pulsing mode at 50 K, with a 200 kHz pulse frequency and 20% voltage pulse fraction. Figure 3B is a 3D map showing Au and Ag atoms indicating the region of Ag-doped Au coating. The Ca isosurface is attributed to the presence of a HAP nanoparticle. The combined information of the interface location and the presence of the nanoparticle here shows that our protocol allows for the substrate/coating interface encapsulation of a nanoparticle sample.

Encapsulated and pre-tilted nanowire

Nanowires are of great interest for advanced small-scale functional devices^[10,26]. Elemental doping in nanowires can have an enormous influence on their electrical functionality. Hence, it is important to understand any chemical heterogeneity induced during doping by advanced characterization techniques such as APT^[10,26]. Traditional free-standing nanowires have a nanoscale needle shape grown out of the substrate a few micrometers in height, catering to the APT specimen requirements of a needle-shape

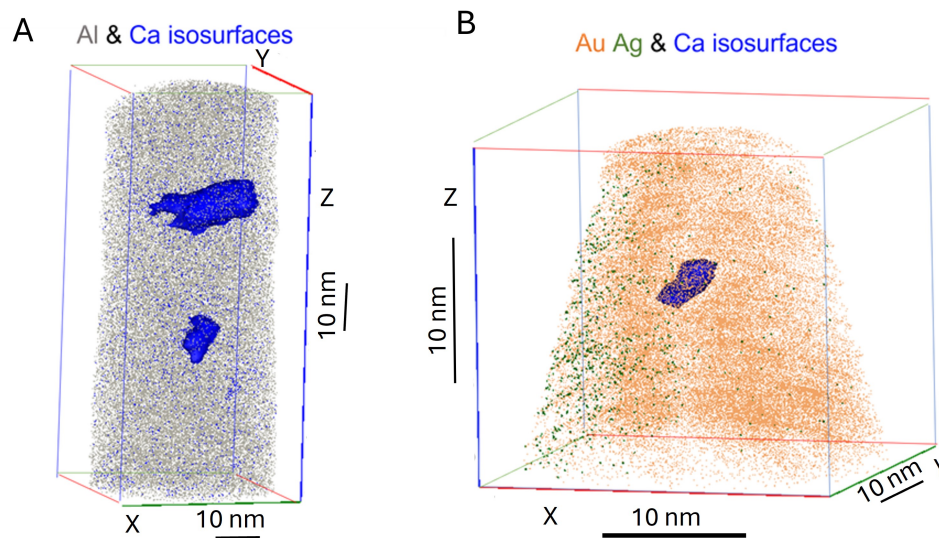


Figure 3. APT data reconstructions of HAP nanoparticle-containing samples. (A) Global view of an Al_2O_3 data reconstruction, showing Al atoms (only 20% are shown for clarity) and 3.4% Ca isosurfaces that show the location of the nanoparticles; (B) Global view of a HAP nanoparticle encapsulated in gold, showing Au (30% shown) and Ag atoms indicating the coating/matrix, as well as 2.6% Ca, indicating the location of a single HAP nanoparticle. APT: Atom probe tomography; HAP: Hydroxyapatite.

specimen with around 100 nm apex. They can be directly measured with APT after mounting appropriately and aligning with the APT optical axis^[10,26]. In contrast, novel planar nanowires have become increasingly popular due to their compatibility with current planar lithographic Si processing technology. This type of planar nanowire grows in the in-plane direction on the substrate. Encapsulation can be used to prepare these samples for atom probe analysis^[11] and this approach can provide a robust specimen structure, leading to more meaningful analyses^[11].

The nanowire specimen presented here is a selective area epitaxial InGaAs nanowire on a GaAs substrate grown via mask-assisted molecular beam epitaxy, with the axial direction parallel to the substrate surface. The outermost In segregation layer is of research interest, with a nominal thickness of ~20 nm, and the APT was used to determine the In composition variation at the outermost layer. However, the very thin InGaAs layer mills quickly under the FIB, and it is extremely challenging to retain the APT tip apex right at the nanowire surface. Therefore, we developed a new strategy to prepare the tip along the nanowire axial direction, allowing the nanowire surface to be collected in the middle of the APT dataset. The nanowire sample was initially encapsulated in a layer of Al by using thermal evaporation. As illustrated in Figure 4A, FIB fabrication started with Pt deposition to protect from ion beam milling. After lifting out the sample containing the nanowire, the manipulator was then rotated 180 degrees in line with the previously described method for aligning the axial direction of the nanowire with a 12-degree pre-tilted pre-sharpened post [Figure 4B]. Figure 4C illustrates the orientation of the specimen from the aspect noted in Figure 4B. As shown in the schematic in Figure 4D, this method creates an angle between the nanowire and the APT tip after attaching the lift-out bar and then normalizing the tilt of the pre-sharpened post. Figure 4E is a SEM image of the illustration in Figure 4D. After rough milling, the nanowire specimen can be targeted as shown in Figure 4F. It is critical that the axial direction of the nanowire is not exactly perpendicular to the APT tip analysis direction. If there is a coincidence between the axial directions of the nanowire and the APT analysis direction it becomes difficult to target the nanowire during annular milling. We have found that the inclined angle plays a significant role in enhancing the overall data yield.

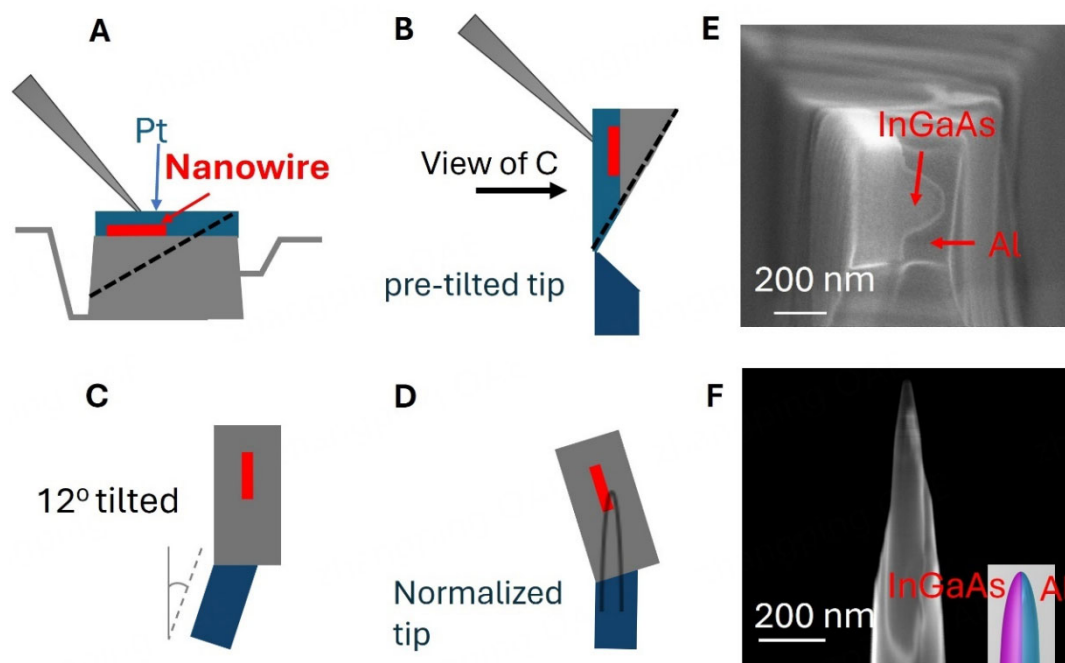


Figure 4. (A) Schematic of a lift-out bar with encapsulated nanowires; (B) Schematic showing the attachment between lifted-out wedge (after 180° rotation of manipulator) and the pre-sharpened post (with a tilt angle of 12° into the paper); (C) The attached tip from the viewing direction indicated in (B); (D) The orientation of the attached tip after the post tilt was normalized; (E) SEM top view image of APT tip, showing nanowire cross-section; (F) The final tip ready for APT measurement after annular milling. The inset shows the geometry of the specimen with half nanowire and half Al capping layer. APT: Atom probe tomography; SEM: Scanning electron microscope.

An inclined nanowire dataset is shown in Figure 5 from a laser-pulsing APT experiment using 20 pJ laser energy, 40 K stage temperature, and 200 kHz pulse frequency. Figure 5A is a desorption map showing the interface between the nanowire and the Al capping layer. Figure 5B is the reconstructed 3D dataset showing the nanowire/matrix interface and a blue ROI used to produce a one-dimensional concentration profile, as shown in Figure 5C. Our method enables intact data collection from the nanowire surface, which offers an opportunity to investigate the In composition in the thin outermost layer. As can be seen in the figure, both Al and the nanowire are present, and their boundary is almost a straight line. This specimen geometry helps to investigate the outermost region of nanowires. Due to the inhomogeneity, the nanowire and Al capping element can have different evaporating properties, leading to trajectory aberrations. However, the current commercial reconstruction algorithms are based on selecting only one primary element. As a result, the data reconstruction fidelity may be influenced by the inhomogeneity structure^[27-29]. It is noted that the main factor determining the accuracy limit of the interfaces is subject to specific reconstruction methodology employed^[30]. In this work, TEM images of nanowire cross-sections were also used to assist with our reconstruction. The results indicate a ~ 94% In: Ga ratio. The ability to characterize the thin surface region of nanowires will allow the correlation of the measured composition with the performance of such materials, leading to an optimal design of the nanomaterials and their fabrication process.

Buried thin-film superlattice

The third specimen is a multilayered thin film which is epitaxial to a ZrN buffer layer on a MgO substrate, as illustrated in Figure 6A. The thin films have multiple periods of 7 nm/7 nm-ZrN/Sc_{0.99}Mg_{0.01}N metal/semiconductor multilayer structure, and the multilayer structure is sandwiched between two ZrN buffers of 0.2 and 1 μm in thickness on the top and bottom, respectively. This material has excellent thermal and

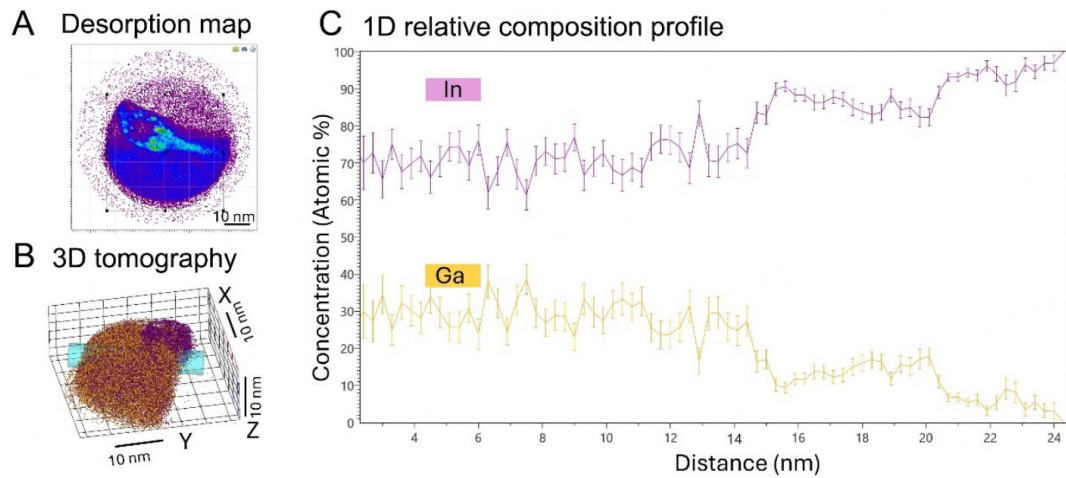


Figure 5. Data reconstruction of an embedded nanowire sample. (A) Desorption map highlighting the nanowire/Al capping layer interface area; (B) reconstructed 3D tomography of nanowire; (C) Atomic concentration 1D profile across the nanowire/Al capping layer interface. 3D: Three-dimensional; 1D: One-dimensional.

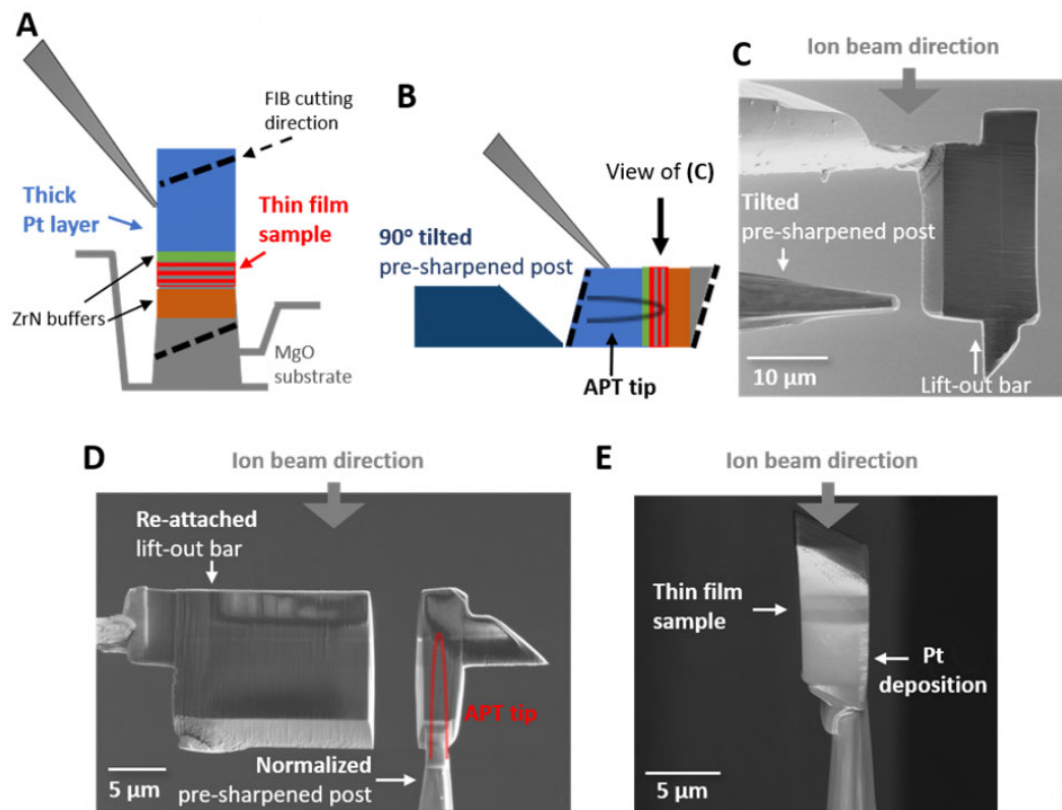


Figure 6. (A) Schematic of the lift-out of a buried thin film; (B) Schematic of the attachment of a rotated lift-out bar with a horizontal pre-sharpened post; (C) SEM image of (B) in the noted viewing direction before attachment; (D) SEM image showing the attachment of a sample bar onto a rotated pre-sharpened post; (E) SEM image of a sample bar incorporating the thin film sample and the Pt deposition. SEM: Scanning electron microscope.

electronic properties useful for thermo-/electro-energy conversion^[31]. The doping of Mg in this material as a p-type impurity is important for achieving desired electronic properties by tuning the Schottky barrier of

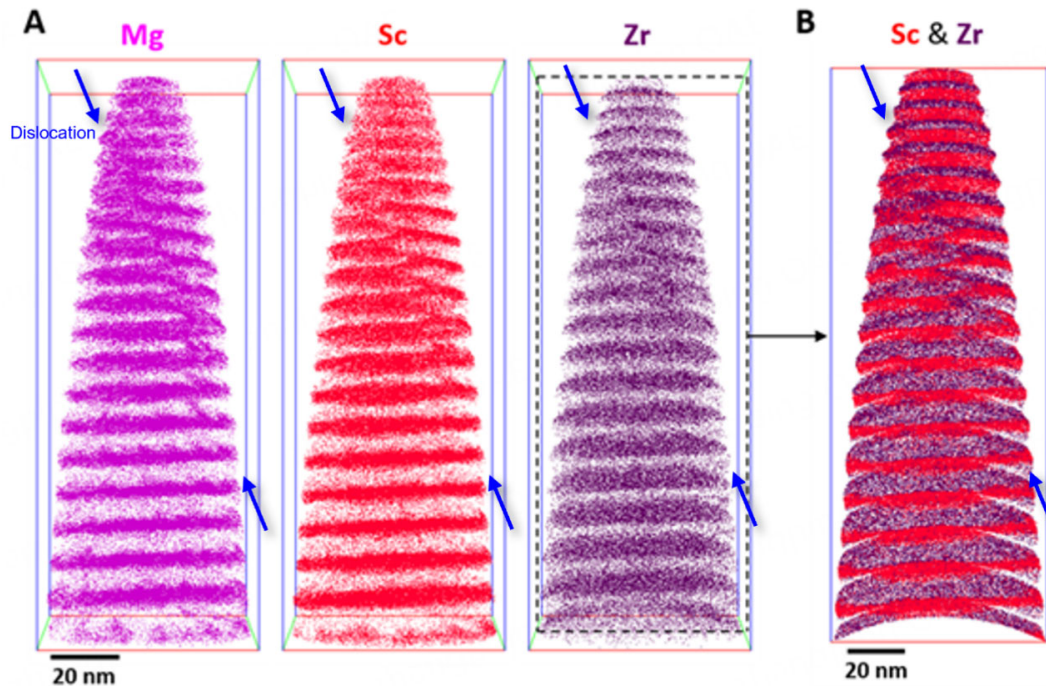


Figure 7. Data reconstruction of a ZrN/Sc_{0.99}Mg_{0.01}N metal/semiconductor multilayer sample. (A) Three-dimensional ion maps of Mg, Sc, and Zr. For clarity, only 3% of atoms of the latter two elements are shown; (B) A 5-nm 'slice' of data showing Sc and Zr, taken from the middle of (A), showing the multilayer structure of this sample. The arrows indicate the location of pipe diffusion through a dislocation.

the multilayer device that contains intrinsic n-type impurities such as oxygen. It is essential to understand how Mg atoms are distributed in this material to optimize the heat treatment parameters in the fabrication of the multilayer device. This information can be obtained using high-resolution elemental mapping via APT.

In order to accurately understand the distribution of Mg within this material and to eliminate potential inaccuracies caused by field effects^[32], a lift-out is required that places the deposition direction perpendicular to the APT analysis direction, which is explained as a backside lift-out^[33]. To achieve this backside lift-out, a thick Pt layer of approximately 5 μm is deposited on the thin ZrN capping layer. In this particular instance, the Pt layer acts as the base of the APT specimen, as opposed to its usual function of protecting the specimen from ion beam damage [Figure 6A and B]. Figure 6A shows the configuration of the trenced bar. Similar to the maneuver conducted for the above two samples, the bar was rotated by 90 degrees, as shown in Figure 6B, enabling alignment and attachment to a 90-degree pre-tilted APT tip post [Figure 6C]. Due to the incident direction of the ion beam indicated in Figure 6C, the orientation of the specimen at this step does not allow specimen shaping by ion beams. It is therefore necessary to first attach the entire backside lift-out bar to the pre-sharpened post and detach the micromanipulator. The stage was then rotated by 90 degrees, the lifted-out bar re-attached to the micromanipulator, followed by the standard attachment of individual bars to the supports, as shown in Figure 6D. As per standard protocols, each bar was then annular milled in preparation for APT analysis [Figure 6E].

The resulting APT tip was tested in laser-pulsing mode at 60 K and 200 kHz pulse frequency with 100 pJ laser energy, leading to the 3D reconstruction shown in Figure 7. Figure 7A contains the 3D atom maps of Mg, Sc, and Zr, whereas Figure 7B is a two-dimensional slice from Figure 7A showing Sc and Zr. The Mg

and Sc maps show the locations of the $\text{Sc}_{0.99}\text{Mg}_{0.01}\text{N}$ layers, whereas the locations of Zr-rich regions correspond to the ZrN interlayers. In this dataset, pipe diffusion of Mg through a dislocation in this superlattice is captured^[34]. This shows how the constituent elements behave during fabrication, providing valuable insight for the future design of this type of multilayered thin film for optimal thermoelectric performance.

CONCLUSIONS

In conclusion, we have highlighted the usefulness and versatility enabled by a rotatable manipulator in the state-of-the-art FIB instrument. This new function directly enables flexible FIB workflows that provide increased throughput and minimize the complexity of the FIB process. Analysis of these materials via APT has been limited by the difficulty of previous FIB sample preparation methods. New simplified lift-out processes will enable a greater quantity of material to be analyzed in the future, providing the capacity for more robust analysis. We anticipate that similar protocols can be applied to research using other advanced microscopy techniques that also involve sophisticated sample preparation.

DECLARATIONS

Acknowledgments

The authors acknowledge the facilities and the scientific and technical assistance of the University of Sydney's Research & Prototype Foundry (RPF) and Microscopy Australia (MA) node (Sydney Microscopy & Microanalysis, SMM), noting financial support from the Australian National Fabrication Facility under the auspices of the National Collaborative Research Infrastructure Strategy program.

Authors' contributions

Contributions to conception and design of the study and performed data analysis and interpretation: Yang, L.; Chen, E. Y. S.; Cairney, J. M.

Performed data acquisition and provided administrative, technical, and material support: Qu, J.; Garbrecht, M.; McCarroll, I. E.; Mosiman, D. S.; Saha, B.

Availability of data and materials

The data are available from the corresponding author upon reasonable request.

Financial support and sponsorship

Mosiman, D. S. acknowledges funding from the American Water Works Association Larson Aquatic Research Support Doctoral Scholarship and the National Science Foundation (NSF) Graduate Research Fellowship Program and Graduate Research Opportunities Worldwide (GROW) Program (DGE-1746047). Chen, E. Y. S. thanks the University of Sydney for its Fellowship support. Saha, B. appreciates the financial backing from the International Centre for Materials Science (ICMS) and Sheikh Saqr Laboratory (SSL) in JNCASR. Cairney, J. M. is grateful for the ARC Future Fellowship (FT180100232). We also extend our gratitude to Microsoft Quantum, the European Research Council (ERC) under Grant No. 716655 (HEMS-DAM), the European Union Horizon 2020 research and innovation program under the Marie Skłodowska-Curie Grant No. 722176.

Conflicts of interest

All authors declared that there are no conflicts of interest.

Ethical approval and consent to participate

Not applicable.

Consent for publication

Not applicable.

Copyright

© The Author(s) 2025.

REFERENCES

1. Miller, M. K.; Russell, K. F.; Thompson, G. B. Strategies for fabricating atom probe specimens with a dual beam FIB. *Ultramicroscopy* **2005**, *102*, 287-98. DOI PubMed
2. Thompson, K.; Lawrence, D.; Larson, D. J.; Olson, J. D.; Kelly, T. F.; Gorman, B. In situ site-specific specimen preparation for atom probe tomography. *Ultramicroscopy* **2007**, *107*, 131-9. DOI PubMed
3. Saxey, D. W.; Cairney, J. M.; McGrouther, D.; Honma, T.; Ringer, S. P. Atom probe specimen fabrication methods using a dual FIB/SEM. *Ultramicroscopy* **2007**, *107*, 756-60. DOI PubMed
4. Gault, B.; Moody, M. P.; Cairney, J. M.; Ringer, S. P. Atom probe microscopy. In: Atom Probe Microscopy. Springer Series in Materials Science. New York: Springer, NY. 2012. pp.299-31. DOI
5. Gault, B.; Chieramonti, A.; Cojocaru-Mirédin, O.; et al. Atom probe tomography. *Nat. Rev. Methods. Primers*. **2021**, *1*, 51. DOI PubMed PMC
6. Geuser F, Gault B. Metrology of small particles and solute clusters by atom probe tomography. *Acta. Materialia*. **2020**, *188*, 406-15. DOI
7. Chen, Y. S.; Lu, H.; Liang, J.; et al. Observation of hydrogen trapping at dislocations, grain boundaries, and precipitates. *Science* **2020**, *367*, 171-5. DOI
8. Prosa, T. J.; Larson, D. J. Modern focused-ion-beam-based site-specific specimen preparation for atom probe tomography. *Microsc. Microanal.* **2017**, *23*, 194-209. DOI PubMed
9. Bas, P.; Bostel, A.; Deconihout, B.; Blavette, D. A general protocol for the reconstruction of 3D atom probe data. *Appl. Surf. Sci.* **1995**, *87-88*, 298-304. DOI
10. Chang, A. S.; Lauhon, L. J. Atom probe tomography of nanoscale architectures in functional materials for electronic and photonic applications. *Curr. Opin. Solid. State. Mater. Sci.* **2018**, *22*, 171-87. DOI
11. Sun, Z.; Hazut, O.; Yerushalmi, R.; Lauhon, L. J.; Seidman, D. N. Criteria and considerations for preparing atom-probe tomography specimens of nanomaterials utilizing an encapsulation methodology. *Ultramicroscopy* **2018**, *184*, 225-33. DOI PubMed
12. Yang, Q.; Danaie, M.; Young, N.; et al. Atom probe tomography of Au-Cu bimetallic nanoparticles synthesized by inert gas condensation. *J. Phys. Chem. C*. **2019**, *123*, 26481-9. DOI
13. Yu, B.; Ayvahi, T.; Raine, E.; et al. Enhanced propylene oxide selectivity for gas phase direct propylene epoxidation by lattice expansion of silver atoms on nickel nanoparticles. *Appl. Catal. B: Environ.* **2019**, *243*, 304-12. DOI
14. Jiang, K.; Back, S.; Akey, A. J.; et al. Highly selective oxygen reduction to hydrogen peroxide on transition metal single atom coordination. *Nat. Commun.* **2019**, *10*, 3997. DOI PubMed PMC
15. Wang, Z.; Li, T.; Jiang, Y.; et al. Acidity enhancement through synergy of penta- and tetra-coordinated aluminum species in amorphous silica networks. *Nat. Commun.* **2020**, *11*, 225. DOI
16. Wilde, P.; Dieckhofer, S.; Quast, T.; et al. Insights into the formation, chemical stability, and activity of transient Ni₃P@NiO_x core-shell heterostructures for the oxygen evolution reaction. *ACS Appl. Energy. Mater.* **2020**, *3*, 2304-9. DOI
17. Lawrence, D.; Alvis, R.; Olson, D. Specimen preparation for cross-section atom probe analysis. *Microsc. Microanal.* **2008**, *14*, 1004-5. DOI
18. Devaraj, A.; Perea, D. E.; Liu, J.; et al. Three-dimensional nanoscale characterisation of materials by atom probe tomography. *Int. Mater. Rev.* **2018**, *63*, 68-101. DOI
19. Eder, K.; Bhatia, V.; Van, L. B.; Cairney, J. M. Using a plasma FIB equipped with Xe, N₂, O₂ and Ar for atom probe sample preparation - ion implantation and success rates. *Microsc. Microanal.* **2019**, *25*, 316-7. DOI
20. Halpin, J. E.; Webster, R. W. H.; Gardner, H.; Moody, M. P.; Bagot, P. A. J.; MacLaren, D. A. An in-situ approach for preparing atom probe tomography specimens by xenon plasma-focussed ion beam. *Ultramicroscopy* **2019**, *202*, 121-7. DOI PubMed
21. Felfer, P.; Li, T.; Eder, K.; et al. New approaches to nanoparticle sample fabrication for atom probe tomography. *Ultramicroscopy* **2015**, *159 Pt 2*, 413-9. DOI
22. Felfer, P.; Benndorf, P.; Masters, A.; Maschmeyer, T.; Cairney, J. M. Revealing the distribution of the atoms within individual bimetallic catalyst nanoparticles. *Angew. Chem. Int. Ed.* **2014**, *53*, 11190-3. DOI PubMed
23. Kim, S. H.; Kang, P. W.; Park, O. O.; et al. A new method for mapping the three-dimensional atomic distribution within nanoparticles by atom probe tomography (APT). *Ultramicroscopy* **2018**, *190*, 30-8. DOI
24. Kim, S. H.; Lee, J. Y.; Ahn, J. P.; Choi, P. P. Fabrication of atom probe tomography specimens from nanoparticles using a fusible Bi-In-Sn alloy as an embedding medium. *Microsc. Microanal.* **2019**, *25*, 438-46. DOI
25. Mosiman, D. S.; Chen, Y. S.; Yang, L.; et al. Atom probe tomography of encapsulated hydroxyapatite nanoparticles. *Small. Methods*. **2021**, *5*, e2000692. DOI

26. Qu, J.; Ringer, S.; Zheng, R. Atomic-scale tomography of semiconductor nanowires. *Mater. Sci. Semicond. Process.* **2015**, *40*, 896-909. [DOI](#)
27. Vurpillot, F.; Larson, D.; Cerezo, A. Improvement of multilayer analyses with a three-dimensional atom probe. *Surf. Interface. Anal.* **2004**, *36*, 552-8. [DOI](#)
28. Brons, J.; Herzing, A.; Henry, K.; Anderson, I.; Thompson, G. Comparison of atom probe compositional fidelity across thin film interfaces. *Thin. Solid. Films.* **2014**, *551*, 61-7. [DOI](#)
29. Op, B. J.; Scheerder, J. E.; Geiser, B. P.; et al. The prospect of spatially accurate reconstructed atom probe data using experimental emitter shapes. *Microsc. Microanal.* **2022**, *28*, 1141-9. [DOI](#)
30. Larson, D. J.; Prosa, T. J.; Geiser, B. P.; Egelhoff, W. F. J. Effect of analysis direction on the measurement of interfacial mixing in thin metal layers with atom probe tomography. *Ultramicroscopy* **2011**, *111*, 506-11. [DOI](#) [PubMed](#)
31. Garbrecht, M.; Mccarroll, I.; Yang, L.; et al. Thermally stable epitaxial ZrN/carrier-compensated Sc_{0.99}Mg_{0.01}N metal/semiconductor multilayers for thermionic energy conversion. *J. Mater. Sci.* **2020**, *55*, 1592-602. [DOI](#)
32. Marquis, E. A.; Geiser, B. P.; Prosa, T. J.; Larson, D. J. Evolution of tip shape during field evaporation of complex multilayer structures. *J. Microsc.* **2011**, *241*, 225-33. [DOI](#) [PubMed](#)
33. Prosa, T.; Lawrence, D.; Olson, D.; Larson, D.; Marquis, E. Backside lift-out specimen preparation: reversing the analysis direction in atom probe tomography. *Microsc. Microanal.* **2009**, *15*, 298-9. [DOI](#)
34. Kumar, R.; Yang, L.; Mccarroll, I.; et al. Atomistic structure and three-dimensional spatial distribution of oxide clusters along voids in nitride metal/semiconductor superlattices. *Phys. Rev. Materials.* **2021**, *5*. [DOI](#)